EFFECTS OF CIRCULAR CORNERS AND ASPECT-RATIO ON ENTROPY GENERATION DUE TO NATURAL CONVECTION OF NANOFLUID FLOWS IN RECTANGULAR CAVITIES

by

Mahmoud SALARI [a*], ***Ali MOHAMMADTABAR*** [b], ***and Mohammad MOHAMMADTABAR*** [c]

[a] Department of Mechanical Engineering, Imam Hussein University, Tehran, Iran
[b] Department of Mechanical Engineering, Azad Islamic University Branch Tehran, Iran
[c] Department of Mechanical Engineering, University of Alberta, Edmonton, Alb., Canada

Original scientific paper
DOI:10.2298/TSCI130201034S

In this paper, entropy generation induced by natural convection of Cu-water nanofluid in rectangular cavities with different circular corners and different aspect-ratios were numerically investigated. The governing equations were solved using a finite volume approach and the SIMPLE algorithm was used to couple the pressure and velocity fields. The results showed that the total entropy generation increased with the increase of Rayleigh number, irreversibility coefficient, aspect ratio or solid volume fraction while it decreased with the increase of the corner radius. It should be noted that the best way for minimizing entropy generation is decreasing Rayleigh number. This is the first priority for minimizing entropy generation. The other parameters such as radius, volume fraction, etc. are placed on the second priority. However, Bejan number had an inverse trend compared with total entropy generation. As an exception, Bejan number and total entropy number had the same trend whenever solid volume fraction increased. Moreover, Nusselt number increased as Rayleigh number, solid volume fraction or aspect ratio increased whereas it decreases with the increase of corner radius.

Key words: *entropy generation, nanofluid, circular corners, rectangular cavity, natural convection, numerical analysis*

Introduction

Natural convention heat transfer has various applications in many practical fields such as cooling system of electronic components, solar collectors, wall insulations, thermal systems of building, and natural circulation in the atmosphere. Minimization of entropy generation is the optimal design criteria for various practical thermal systems such as electronic cooling, turbo-machines, heat exchangers, *etc.* Bejan [1] showed that flow parameters should be designed to minimize the irreversibility related to a specific convective heat transfer. Abu-Hijleh *et al.* [2] numerically studied the entropy generation of natural convection in a horizontal cylinder. They showed, for a range of Rayleigh numbers, entropy generation decreased with the increase of the cylinder diameter. Zahmatkesh [3] investigated entropy generation of natural convection in a porous enclosure and indicated that the generation rate was maximum

* Corresponding author; e-mail: m_salari@iust.ac.ir, msalari@ihu.ac.ir

for uniform heating/cooling and minimum for non-uniform heating/cooling. Olivesli *et al.* [4] considered entropy generation in a rectangular cavity which was submitted to a horizontal temperature gradient and showed variation of entropy generation in relation to Rayleigh number, aspect ratio and irreversibility coefficient. Salari *et al.* [5] studied numerical study of entropy generation for natural convection in rectangular cavity with circular corners. Khanatee *et al.* [6] introduced a new class of fluid with higher thermal conductivity and called it nanofluids which consisted of suspended nanoparticles with better suspension stability compared with millimeter and micrometer sized particles. Natural convection of different nanofluids in cavity has been numerically carried out by many investigators [7-13]. Feng and Kleinstrener [14] studied entropy generation of nanofluids flow between parallel disks. Li and Kleinstrener [15] analyzed entropy generation in trapezoidal microchannels when the used nanofluids were a combination of water and CuO nanoparticles. They determined the most suitable channel aspect ratio and Reynolds number range by minimizing entropy generation. Singh *et al.* [16] studied entropy generation in micro-channel, mini-channel and a conventional channel with alumina-water nanofluids. They reported an optimum diameter for minimizing entropy generation rate. Mahmoudi *et al.* [17] simulated a numerical study of entropy generation in a square open cavity heated with a protruded heat source and showed that the position of open boundary and location of the heater had considerable effects on heat transfer characteristics and irreversibility. The entropy generation due to flow and heat transfer of nanofluids between co-rotating cylinders with constant heat flux on the walls is studied analytically by Mahian *et al.* [18]. In other work, the mixed convection flow between two vertical concentric pipes with constant heat flux at the boundaries and MHD flow effects is considered by Mahian *et al.* [19]. In the study by Selimefendigil and Oztop [20], a square cavity with two ventilation ports in the presence of an adiabatic fin of different lengths placed on the walls of the cavity is numerically analyzed for the mixed convection case. Also a good review about the entropy generation due to flow and heat transfer of nanofluids in different geometries and flow regimes is presented by Mahian *et al.*[21]. The objective of this work is to investigate entropy generation due to natural convection in a rectangular cavity with different circular corners. Based on the knowledge of authors, there has been no paper on the effects of circular corners on Nusselt number and total entropy generation. This paper presents dependence of total entropy generation, Bejan number and Nusselt number on various parameters such as Rayleigh number, solid volume fraction, aspect ratio and corner radius.

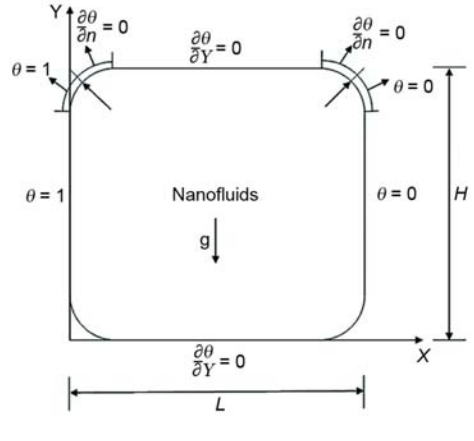

Figure 1. Physical model and co-ordinate system

Mathematical model

Geometry of the enclosure considered in this paper is shown in fig. 1. Left and right walls are kept at constant temperature of T_h and T_c, respectively. Top and bottom walls are assumed adiabatic. All the corners are divided into two parts. The part linked to top or bottom walls is assumed to be adiabatic while the other part which is connected to left or right walls is kept at the same temperature with those walls. The flow of nanofluid within the enclosure is assumed to be laminar, Newtonian, and incompressible. Moreover, solid nanoparticles and base fluid are in the thermal equilibrium. Thermo-physical properties of nanofluid are constant, except the density obtained by the assumption of Boussinesq approximation. Table 1 [16, 22] shows properties of the base fluid and diverse nanoparticles used in this paper at reference temperature 25 °C. However, at the procedure of computation and for each computation cell all the parameters presented at tab. 1 are depending on temperature and their amounts are updated for each cell.

Table 1. Thermo-physical properties of water and nanoparticles [22]

	ρ [kgm^{-3}]	C_p [Jkg^{-1}K^{-1}]	k [Wm^{-1}K^{-1}]	$\beta \cdot 10^5$ [K^{-1}]
Pure water	997.1	4179	0.613	21
Copper	8933	385	401	1.67

The governing equations of continuity, momentum, and energy with the assumptions can be obtained:

$$\frac{\partial u}{\partial x}+\frac{\partial v}{\partial y}=0 \tag{1}$$

$$u\frac{\partial u}{\partial x}+v\frac{\partial u}{\partial y}=\frac{1}{\rho_{\mathrm{nf}}}\left[-\frac{\partial p}{\partial x}+\mu_{\mathrm{nf}}\left(\frac{\partial^2 u}{\partial x^2}+\frac{\partial^2 u}{\partial y^2}\right)\right] \tag{2}$$

$$u\frac{\partial v}{\partial x}+v\frac{\partial v}{\partial y}=\frac{1}{\rho_{\mathrm{nf}}}\left[-\frac{\partial p}{\partial y}+\mu_{\mathrm{nf}}\left(\frac{\partial^2 v}{\partial x^2}+\frac{\partial^2 v}{\partial y^2}\right)+(\rho\beta)_{\mathrm{nf}}\,g(T-T_{\mathrm{c}})\right] \tag{3}$$

$$u\frac{\partial T}{\partial x}+v\frac{\partial T}{\partial y}=\alpha_{\mathrm{nf}}\left(\frac{\partial^2 T}{\partial x^2}+\frac{\partial^2 T}{\partial y^2}\right) \tag{4}$$

The effective density of nanofluid can be achieved:

$$\rho_{\mathrm{nf}}=(1-\phi)\rho_{\mathrm{f}}+\phi\rho_p \tag{5}$$

where ϕ is the solid volume fraction of nanofluid.

Thermal diffusivity of nanofluid is determined:

$$\alpha_{\mathrm{nf}}=\frac{k_{\mathrm{nf}}}{(\rho C_p)_{\mathrm{nf}}} \tag{6}$$

Heat capacity of the nanofluid is obtained:

$$(\rho C_p)_{\mathrm{nf}}=(1-\phi)(\rho C_p)_f+\phi(\rho C_p)_p \tag{7}$$

Also, the thermal expansion coefficient of the nanofluid is expressed:

$$(\rho\beta)_{\mathrm{nf}}=(1-\phi)(\rho\beta)_f+\phi(\rho\beta)_p \tag{8}$$

The effective dynamic viscosity of the nanofluid presented by Brinkman [23] is given:

$$\mu_{\rm nf} = \frac{\mu_{\rm f}}{(1-\phi)^{2.5}} \tag{9}$$

The effective thermal conductivity of the nanofluid calculated by Abu-Nada and Chamkha [24] is:

$$\frac{k_{\rm nf}}{k_{\rm f}} = 1 + 64.7\ \phi^{0.7640} \left(\frac{d_{\rm f}}{d_{\rm p}}\right)^{0.3690} \left(\frac{k_{\rm f}}{k_{\rm p}}\right)^{0.7476} \mathrm{Pr}_{\rm T}^{0.9955} \mathrm{Re}^{1.2321} \tag{10}$$

where $k_{\rm f}$ is the thermal conductivity of pure fluid and $k_{\rm p}$ is the thermal conductivity of dispersed nanoparticles. $\mathrm{Pr}_{\rm T}$ and Re are defined:

$$\mathrm{Pr}_{\rm T} = \frac{\mu_{\rm f}}{\rho_{\rm f}\alpha_{\rm f}} \tag{10-1}$$

$$\mathrm{Re} = \frac{\rho_{\rm f} k_b T}{3\pi\mu_{\rm f}^2 l_{\rm f}} \tag{10-2}$$

The symbol k_b is the Boltzmann constant = $1.3807\cdot10^{-23}$ J/K, and $l_{\rm f}$ – the mean path of fluid practices given as 0.17 nm [24].

The mentioned governing equations are converted to the following dimensionless form by introducing the dimensionless parameters:

$$X = \frac{x}{L}, \quad Y = \frac{y}{L}, \quad U = \frac{uL}{\alpha}, \quad V = \frac{vL}{\alpha}, \quad \theta = \frac{T - T_{\rm c}}{T_{\rm h} - T_{\rm c}}, \quad P = \frac{pL^2}{\rho_{\rm nf}\alpha^2},$$
$$\Delta T = T_{\rm h} - T_{\rm c}, \quad \mathrm{Ra} = \frac{g\beta_{\rm f} L^3 \Delta T}{\upsilon_{\rm f}\alpha_{\rm f}}, \quad \mathrm{Pr} = \frac{\upsilon_{\rm f}}{\alpha_{\rm f}} \tag{11}$$

Using these dimensionless parameters, the governing eqs. (1)-(4) could be written:

$$\frac{\partial U}{\partial X} + \frac{\partial V}{\partial Y} = 0 \tag{12}$$

$$U\frac{\partial U}{\partial X} + V\frac{\partial U}{\partial Y} = -\frac{\partial P}{\partial X} + \frac{\rho_{\rm f}}{\rho_{\rm nf}} \frac{\mathrm{Pr}}{(1-\phi)^{2.5}} \left(\frac{\partial^2 U}{\partial X^2} + \frac{\partial^2 U}{\partial Y^2}\right) \tag{13}$$

$$U\frac{\partial V}{\partial X} + V\frac{\partial V}{\partial Y} = -\frac{\partial P}{\partial Y} + \frac{\rho_{\rm f}}{\rho_{\rm nf}} \frac{\mathrm{Pr}}{(1-\phi)^{2.5}} \left(\frac{\partial^2 V}{\partial X^2} + \frac{\partial^2 V}{\partial Y^2}\right) + \frac{(\rho\beta)_{\rm nf}}{\rho_{\rm nf}\beta_{\rm f}} \mathrm{Ra}\ \mathrm{Pr}\ \theta \tag{14}$$

$$U\frac{\partial \theta}{\partial X} + V\frac{\partial \theta}{\partial Y} = \frac{\alpha_{\rm nf}}{\alpha_{\rm f}} \left(\frac{\partial^2 \theta}{\partial X^2} + \frac{\partial^2 \theta}{\partial Y^2}\right) \tag{15}$$

The dimensionless form of boundary conditions is also expressed:

$X = 0$, on left wall: $U = V = 0,\ \theta = 1$,
$X = 0$, on half parts of corner radii linked to left wall: $U = V = 0,\ \theta = 1$,
$X = 1$, on right wall: $U = V = 0,\ \theta = 0$,
$X = 1$, on half parts of corner radii linked to right wall: $U = V = 0,\ \theta = 0$, (16)
$Y = 0$, on bottom wall: $U = V = 0,\ \partial\theta/\partial Y = 0$,
$Y = 1$, on top wall: $U = V = 0,\ \partial\theta/\partial Y = 0$,
on half parts of corner radii linked to top and bottom walls: $U = V = 0,\ \partial\theta/\partial n = 0$

The local Nusselt number of the nanofluid on left wall can be determined:

$$\mathrm{Nu}_\mathrm{l} = \frac{hL}{k_\mathrm{f}} \tag{17}$$

The convection heat transfer coefficient h is also obtained by:

$$h = \frac{q''}{T_\mathrm{h} - T_\mathrm{c}} \tag{18}$$

and the average Nusselt number (Nu_m) can be achieved by integrating the local Nusselt number (Nu_S) along the heat source:

$$\mathrm{Nu}_m = \frac{1}{H}\int_0^H \mathrm{Nu}_\mathrm{l}(Y)\mathrm{d}Y \tag{19}$$

In the natural convection process the entropy generation is associated with the heat transfer and to the fluid flow friction. The entropy generation for an incompressible flow system was previously developed by Bejan [25]. The volumetric entropy generation in flow, due to the heat transfer and fluid friction, can be written:

$$\dot{S}_\mathrm{l} = \dot{S}_\mathrm{l,h} + \dot{S}_\mathrm{l,f} \tag{20}$$

The heat transfer contribution of the volumetric entropy generation of the nanofluid in a system of 2-D flow is:

$$\dot{S}_\mathrm{l,h} = \frac{K_\mathrm{nf}}{T_0^2}\left[\left(\frac{\partial T}{\partial x}\right)^2 + \left(\frac{\partial T}{\partial y}\right)^2\right] \tag{21}$$

where $T_o = (T_\mathrm{h} + T_\mathrm{c})/2$ is the bulk temperature, and k_nf – the thermal conductivity of nanofluid.

The fluid friction contribution of the volumetric entropy generation of the nanofluid in a system of 2-D flow is determined:

$$\dot{S}_\mathrm{l,f} = \frac{\mu_\mathrm{nf}}{T_0}\left[2\left(\frac{\partial u}{\partial x}\right)^2 + 2\left(\frac{\partial v}{\partial y}\right)^2 + \left(\frac{\partial u}{\partial y} + \frac{\partial v}{\partial x}\right)^2\right] \tag{22}$$

where μ_nf is the dynamic viscosity of nanofluid.

These equations in dimensionless form for the nanofluid can be determined:

$$\dot{S}_{\mathrm{l},a} = \dot{S}_{\mathrm{l},a,\mathrm{h}} + \dot{S}_{\mathrm{l},a,\mathrm{f}} \tag{23}$$

$$\dot{S}_{\mathrm{l},a,\mathrm{h}} = \frac{K_\mathrm{nf}}{K_\mathrm{f}}\left[\left(\frac{\partial\theta}{\partial X}\right)^2 + \left(\frac{\partial\theta}{\partial Y}\right)^2\right] \tag{24}$$

$$\dot{S}_{\mathrm{l},a,\mathrm{f}} = \frac{\varphi}{(1-\phi)^{2.5}}\left[2\left(\frac{\partial U}{\partial X}\right)^2 + 2\left(\frac{\partial V}{\partial X}\right)^2 + \left(\frac{\partial U}{\partial Y} + \frac{\partial V}{\partial X}\right)^2\right] \tag{25}$$

where φ is the ratio between viscous and thermal irreversibility and is defined:

$$\varphi = \frac{\mu_\mathrm{f} T_0}{k_\mathrm{f}}\left[\frac{\alpha_\mathrm{f}}{L(T_\mathrm{h} - T_\mathrm{c})}\right]^2 \tag{26}$$

The dimensionless total entropy generation of the nanofluid is achieved by getting integral over the entire volume of the dimensionless local entropy generation:

$$\dot{S}_{T,a} = \int \dot{S}_{\mathrm{l},a}\,\mathrm{d}\,v \tag{27}$$

The Bejan non-dimensional number of the nanofluid (Be) is also expressed:

$$\mathrm{Be} = \frac{\dot{S}_{\mathrm{l},a,\mathrm{h}}}{\dot{S}_{\mathrm{l},a}} \tag{28}$$

Grid generation

Figure 2 schematically shows grid generation processes, which was done according to the following steps:

– a structured grid was generated algebraically for the rectangular cavity (first, without considering the circular corners). Accordingly, all cell geometries had a rectangular form. Clustering could be also used near the cavity walls,

– the rectangular cells in vicinity of the circular boundaries were totally selected as computational domain (*i. e.* where their pieces were placed in the physical domain). Then, the remaining cells between circular corner and the rectangular cavity walls were withdrawn, and the required boundary condition could be imposed to the extra cell boundaries, (fig. 2).

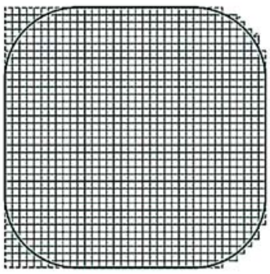

Figure 2. Structured grid features

It can be seen in fig. 2 that the circular boundaries were approximated with broken lines. However, this error can be reduced by decreasing mesh sizes.

Numerical method and validation

The non-dimensional governing eqs. (12)-(15) were numerically solved based on the finite volume approach presented by Patankar [26]. For coupling the pressure and velocity fields, the SIMPLE algorithm was applied. A non-uniform grid mesh which was thinner in the vicinity of walls was used to increase accuracy of the results. The effect of grid resolution was studied in order to find suitable grid density. The results of the grid study on average Nusselt number are reported in tab. 2. Based on the results presented in this table, a 100 × 100 non-uniform grid was selected for the numerical simulation of this research. The convergence

Table 2. Grid study results (Cu-water, A = 1, r = 0.3, ϕ = 0.1, φ = 10^{-2}, Ra = 10^5)

Grid	25 × 25	50 × 50	75 × 75	100 × 100	125 × 125
Nu	2.5532	2.4815	2.4782	2.4767	2.4765
$\lvert\psi_{\max}\rvert$	6.9479	6.5917	6.5971	6.5972	6.5972

criteria were satisfied when maximum mass residuals of the grid control volume was less than about 10^{-9}. For validation of the present numerical code, U velocity profile of a mixed convection flow within a lid-driven square enclosure obtained by this code was compared with that of the numerical results presented by several investigators [27-29]. As shown in fig. 3, these results were in good agreement with each other. Moreover, the results of averaged Nusselt number in this research were compared with those presented by Oliveski *et al.*, [4] and Davis de Vahl [30], as shown in tab. 3. In addition, tab. 4 shows the comparison of non-dimensional total entropy generation ($\dot{S}_{Ta}$) obtained by this code with other investigations [4, 31]. Both tabs. 3 and 4 demonstrate that both average Nusselt number and non-dimensional total entropy generation obtained by the present numerical code had very good agreement with the results presented by other investigators.

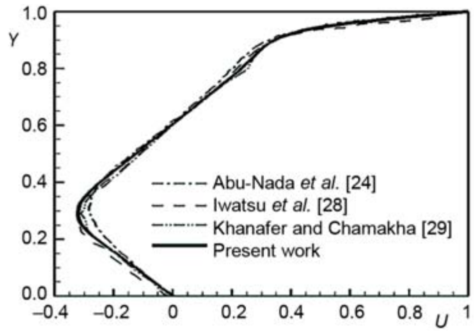

Figure 3. Comparision of the *U*-velocity profile of the present study with those of the other investigators [27-29]

Table 3. The comparison of averaged Nusselt number of present study with others

	Ra = 10^3		Ra = 10^4		Ra = 10^5		Ra = 10^6	
	$\lvert\psi_{max}\rvert$	Nu	$\lvert\psi_{max}\rvert$	Nu	$\lvert\psi_{max}\rvert$	Nu	$\lvert\psi_{max}\rvert$	Nu
Oliveski *et al.* [4]	1.183	1.118	5.533	2.243	11.99	4.519	32.97	8.800
de Vahl Davis [30]	1.181	1.116	5.529	2.239	11.97	4.531	32.93	8.721
Present work (r = 0)	1.184	1.117	5.532	2.244	12.01	4.522	32.99	8.830
The difference with Oliveski *et al.* [4] [%]	0.08	0.09	0.02	0.04	0.16	0.07	0.06	0.34
The difference with Davis de Vahl [30] [%]	0.25	0.09	0.05	0.22	0.33	0.2	0.18	1.23

Results and discussion

Table 4. The comparison of total entropy generation of present study with others

	Ra = 10^3, $\varphi = 10^{-2}$	Ra = 10^5, $\varphi = 10^{-4}$
Oliveski *et al.* [4]	4.557	22.863
Magherbi [31]	4.558	22.863
Present work (r = 0)	4.559	22.865

Entropy generation, due to natural convection in a rectangular cavity with circular corners filled by Cu-water nanofluid is numerically studied for a range of solid volume fraction [29, 32] ($0 \leq \phi \leq 0.1$), Rayleigh number ($10^3 \leq \mathrm{Ra} \leq 10^6$), aspect ratio ($1 \leq A \leq 4$), irreversibility coefficient ($10^{-4} \leq \varphi \leq 10^{-2}$), and corner radius ($0 \leq r \leq 0.5$).

Figure 4 shows the effects of different Rayleigh numbers and corner radii on isotherms. Isotherm lines are parallel whenever Rayleigh number is 1000 which mean conduction is dominant. When Rayleigh number increases, the isotherm lines would be distorted. Dimensionless temperature increased with augmenting Rayleigh number while it decreased with increase of the corner radius. Also two last rows show the percent difference of existing data in table 3 between present paper from Davis de Vahl [30] and Oliveski *et al.* [4] which show a good accuracy.

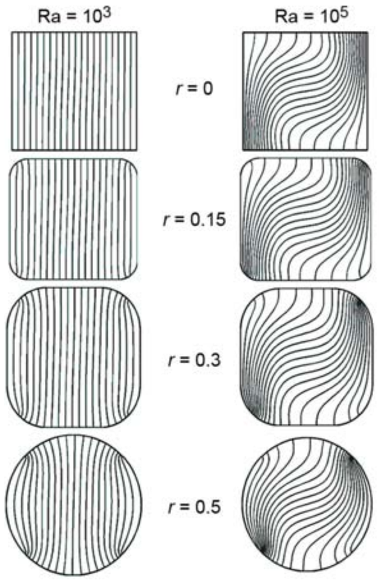

Figure 4. Isotherms for enclosures filled with nanofluid Cu-water at different Rayleigh numbers and corner radii ($\varphi = 10^{-2}$, $\phi = 0.1$, $A = 1$)

Figure 5 illustrates effects of different corner radii on total entropy generation. As shown in the figure, total entropy generation increased with augmenting Rayleigh number. The behavior of total entropy generation, due to corner radii, was rather vague. For showing the behavior, another co-ordinate system was used, which was located on the right side. This axis was called decrease of percent of $\dot{S}_{\mathrm{T}}$ which presented the difference between all the cases, except first case. Using this axis, it is clear that total entropy generation decreased as corner radius was enhanced. Figure 6 presents effects of different solid volume fractions on total entropy generation. Total entropy generation increased by augmenting solid volume fraction. The right axis was called increase of percent of $\dot{S}_{\mathrm{T},a}$ which showed the percent of increase between all the cases, except first case. This behavior was expectable because, by adding more nanoparticles, solid volume fraction increased and it was directly proportional to total entropy generation, as shown in eq. (22).

Figure 7 indicates effects of different irreversibility ratios on total entropy generation. It is obvious that total entropy generation was enhanced as irreversibility ratio augmented. Figure 8 demonstrates effects of different aspect ratios on total entropy generation. As shown in this figure, total entropy generation increased by increasing aspect ratio.

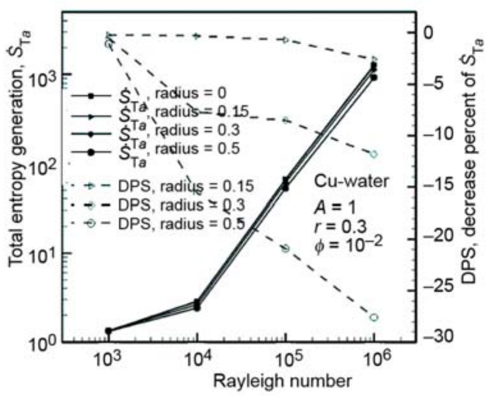

Figure 5. Effects of different corner radii on total entropy generation

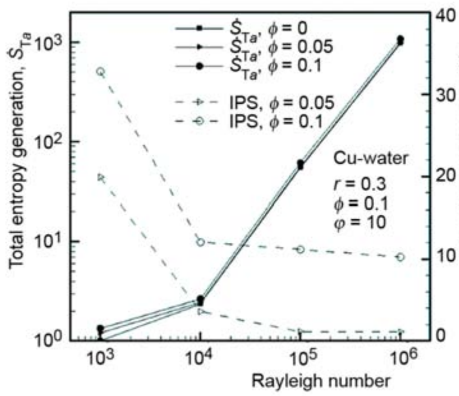

Figure 6. Effects of different solid volume fractions on total entropy generation

Figure 9 presents effects of different corner radii on Bejan number. As shown in fig. 8, it is clear that Bejan number decreased by increasing Rayleigh number. Whenever Rayleigh number increased, heat transfer increased; so dimensionless temperature decreased, then it caused Bejan number to decrease. Moreover, using, increase of percent of Bejan number (IPB), it is obvious that Bejan number increased as corner radius was enhanced. Also, the percent of this increase was augmented by increasing Rayleigh number. Figure 10 shows that

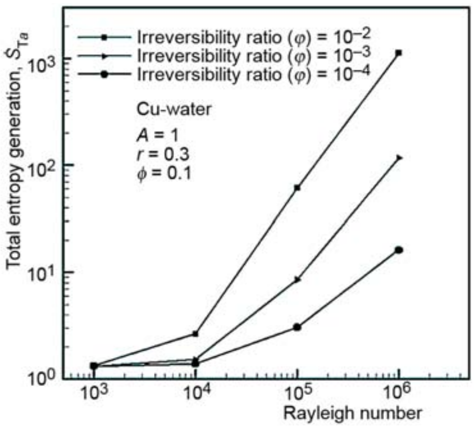

Figure 7. Effects of different irreversibility ratios on total entropy generation

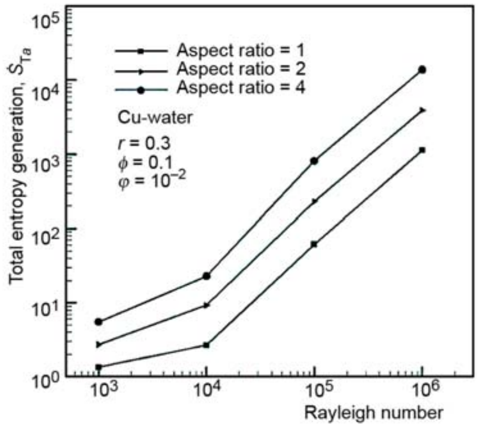

Figure 8. Effects of different aspect ratios on total entropy generation

Bejan number increased as solid volume fraction increased. For better understanding, IPB was also depicted. Figure 11 illustrates that Bejan number decreased by boosting irreversibility ratio. Figure 12 demonstrates that Bejan number decreased as aspect ratio increased. Whenever aspect ratio increased, Nusselt number increased; so, dimensionless temperature decreased and then caused Bejan number to decrease.

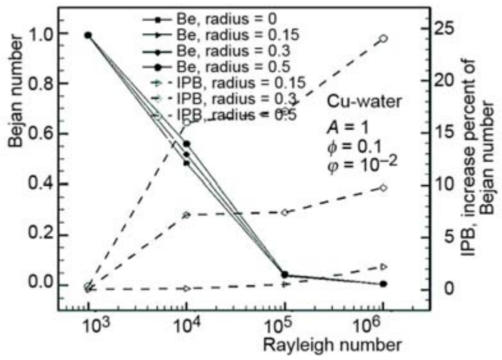

Figure 9. Effects of different corner radii on Bejan number

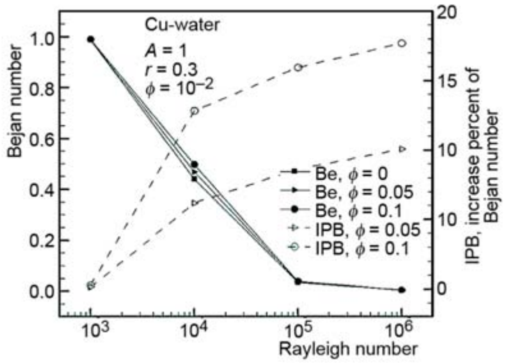

Figure 10. Effects of different solid volume fractions on Bejan number

Figure 13 presents effects of different corner radii on Nusselt number. Using decrease of percent of Nu (DPN), it is clear that Nusselt number decreased as corner radius increased. The percent of this decreasing was enhanced by augmenting Rayleigh number. Figure 14 shows that Nusselt number increased whenever solid volume fraction was augmented. In fig. 15, effects of different aspect ratios on Nusselt number is depicted. Nusselt number was boosted by increasing aspect ratio.

Conclusions

Entropy generation, due to natural convection in a rectangular cavity with different circular corners filled by Cu-water nanofluid, was numerically investigated. Summary of the obtained results are listed:

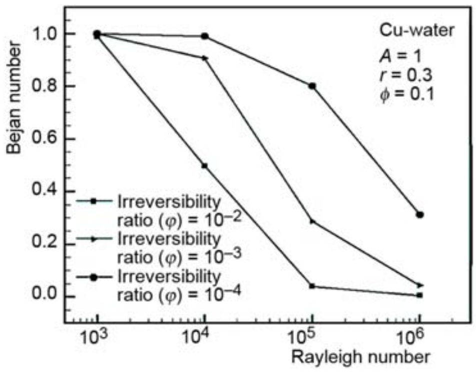

Figure 11. Effects of different irreversibility ratios on Bejan number

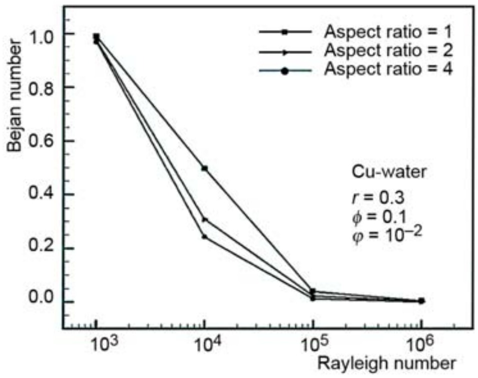

Figure 12. Effects of different aspect ratios on Bejan number

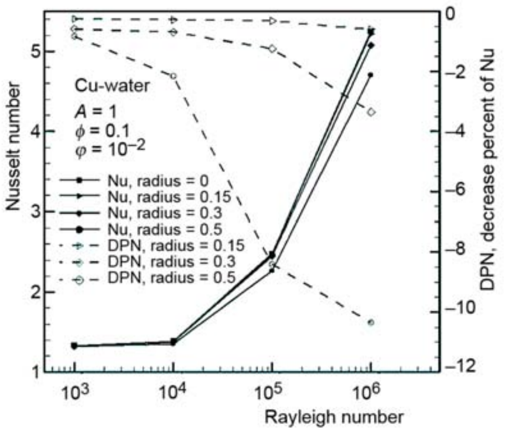

Figure 13. Effects of different corner radii on Nusselt number

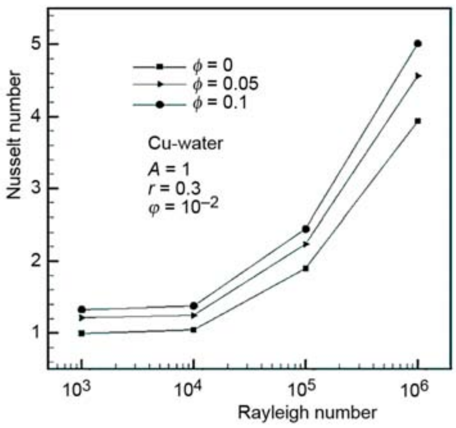

Figure 14. Effects of different solid volume fractions on Nusselt number

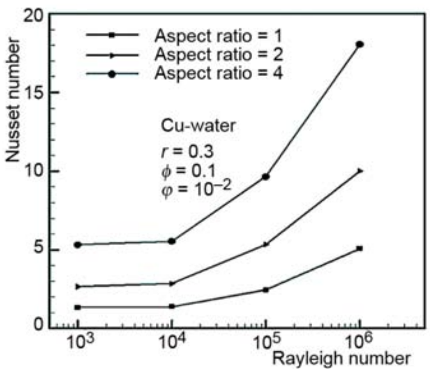

Figure 15. Effects of different aspect ratios on Nusselt number

- Total entropy generation increased by augmenting Rayleigh number, irreversibility coefficient, aspect ratio or solid volume fraction while it decreased with the increase of corner radius. It should be noted that the best way for minimizing entropy generation is decreasing Rayleigh number. This is the first priority for minimizing entropy generation. The other parameters such as radius, volume fraction, *etc.* are placed on the second priority.
- Bejan number was enhanced by augmenting corner radius or solid volume fraction while it decreased by boosting Rayleigh number, irreversibility coefficient or aspect ratio.

- Nusselt number was an increasing function with the increase in Rayleigh number, solid volume fraction or aspect ratio while it was a decreasing function whenever corner radius was enhanced.
- The percent of decreasing of total entropy generation and Nusselt number and the percent of increasing of Bejan number via corner radius increased by augmenting Rayleigh number. Stream function and dimensionless pressure increased by augmenting Rayleigh number while dimensionless temperature decreased. However, by boosting corner radius, stream function and dimensionless pressure were a decreasing function while dimensionless temperature was an increasing one.

Nomenclature

A – aspect ratio, (= H/L)
Be – Bejan number, (= $\dot{S}_{l,a,h}/\dot{S}_{l,a}$)
C_p – specific heat, [$\text{Jkg}^{-1}\text{K}^{-1}$]
d – diameter, [m]
g – gravitational acceleration, [ms^{-2}]
H – height of cavity, [m]
h – heat transfer coefficient, [$\text{Wm}^{-2}\text{K}^{-1}$]
k – thermal conductivity, [$\text{Wm}^{-1}\text{K}^{-1}$]
L – length of cavity, [m]
Nu – Nusselt number
P – dimensionless pressure (= $p/p_{\text{nf}}U_0^2$)
Pr – Prandtl number (ν_f/α_f)
p – pressure, [Pa]
Ra – Rayleigh number (= $gB_f L^3 \Delta T/\nu_f \alpha_f$)
r – dimensionless radius [–]
$\dot{S}$ – entropy generation, [$\text{Wm}^{-3}\text{K}^{-1}$]
T – temperature, [K]
T_o – bulk temperature, [K]
U, V – dimensionless velocity components (= u/U_0, v/U_0)
u, v – velocity components in x-, y-directions, [ms^{-1}]
X, Y – dimensionless co-ordinates (= x/H, y/H)
x, y – Cartesian co-ordinates, [m]

Greek symbols

α – thermal diffusivity, (= $k/\rho C_p$), [m^2s^{-1}]
β – thermal expansion coefficient, [K^{-1}]
θ – dimensionless temperature, [= $(T - T_c)/(T_h - T_c)$]
μ – dynamic viscosity, [$\text{kgm}^{-1}\text{s}^{-1}$]
υ – kinematic viscosity, (μ/ρ), [m^2s^{-1}]
ρ – density, [kgm^{-3}]
ϕ – solid volume fraction
φ – irreversibility, $\{(\mu T_0/k)[\alpha/L(T_h - T_c)]^2\}$
ψ – stream function

Subscripts

a – dimensionless
c – cold
f – pure fluid
h – hot
l – local
nf – nanofluid
p – solid particle
T – total

References

[1] Bejan, A., A Study of Entropy Generation in Fundamental Convective Heat Transfer, *ASME J. Heat Transfer, 101* (1979), 4, pp. 718-725
[2] Abu-Hijleh, B. A. K., *et al.*, Numerical Prediction of Entropy Generation due to Natural Convection from a Horizontal Cylinder, *Energy, 24* (1999), 4, pp. 327-333
[3] Zahmatkesh, I., On the Importance of Thermal Boundary Conditions in Heat Transfer and Entropy Generation for Natural Convection Inside a Porous Enclosure, *Int. J. Therm. Sci., 47* (2008), 3, pp. 339-346
[4] Oliveski, D. C., *et al.*, Entropy Generation and Natural Convection in Rectangular Cavities, *Applied Thermal Eng., 29* (2009), 8-9, pp. 1417-1425
[5] Salari, M., *et al.*, Numerical Study of Entropy Generation for Natural Convection in Rectangular Cavity with Circular Corners, *Heat Transfer Engineering, 36* (2014), 2, pp. 186-199
[6] Khanafer, K., *et al.*, Buoyancy Driven Heat Transfer Enhancement in a Two-Dimensional Enclosure Utilizing Nanofluids, *Int. J. Heat Mass Trans., 4*6 (2001), 19, pp. 3639-3653
[7] Aminossadati, S. M., Ghasemi, B., Natural Convection Cooling of a Localized Heat Source at the Bottom of a Nanofluid-Filled Enclosure, *European Journal of Mechanics-B/Fluids 28* (2009), 5, pp. 630-640
[8] Ghasemi, B., Aminpssadati, S. M., Periodic Natural Convection in a Nanofluid-Filled with Oscillating Heat Flux, *International Journal of Thermal Science 49* (2010), 1, pp. 1-9
[9] Ghasemi, B., Aminossadati, S. M., Natural Convection Heat Transfer in an Inclined Enclosure Filled with a Water-CuO Nanofluid, *Num. Heat Tran., Part A: Applications, 55* (2009), 8, pp. 807-823

[10] Mahmoudi, A. H., *et al.*, Numerical Study of Natural Convection Cooling of Horizontal Heat Source Mounted in a Square Cavity Filled with Nanofluid, *Int. Comm. Heat Mass Transfer, 37* (2010), 8, pp. 1135-1141
[11] Alloui, Z., *et al.*, Natural Convection of Nanofluids in a Shallow Cavity Heated from Below, *Int. J. Therm. Sci., 50* (2011), 3, pp. 385-393
[12] Sheikhzadeh, G. A., *et al.*, Natural Convection of Cu-Water Nanofluid in a Cavity with Partially Active Side Walls, *Eur. J. Mech. B/Fluids 30* (2011), 2, pp. 166-176
[13] Mahmoudi, A. H., *et al.*, Modeling of Conjugated Heat Transfer in a Thickwalled Enclosure Filled with Nanofluid, *Int. Commu. Heat Mass Trans., 38* (2011), 1, pp. 119-127
[14] Feng, Y., Kleinstreuer, C., Nanofluid Convective Heat Transfer in a Parallel-Disk System, *Int .J. Heat Mass Trans., 53* (2010), 21, pp. 4619-4628
[15] Li, J., Kleinstreuer, C., Entropy Generation Analysis for Nanofluid Flow in Microchannels, *J. Heat Trans., 132* (2010), 12, pp. 122401.1-122401.8
[16] Singh, P. K., *et al.*, Entropy Generation due to Flow and Heat Transfer in Nanofluids, *Int. J. Heat Mass Transfer, 53* (2010), 21, pp. 4757-4767
[17] Mahmoudi, A. H., *et al.*, Entropy Generation Due to Natural Convection in a Partially Open Cavity with a Thin Heat Source Subjected to a Nanofluid, *Num. Heat Transfer, Part A, 61* (2012), 4, pp. 283-305
[18] Mahian, O., *et al.*, Analysis of Entropy Generation between Co-Rotating Cylinders using Nanofluids, *Energy*, 44 (2012), 1, pp. 430-446
[19] Mahian, O., *et al.*, Design of a Vertical Annulus With MHD Flow using Entropy Generation Analysis, *Thermal Science*, *17*, (2013), 4, pp. 1013-1022
[20] Selimefendigil, F., Oztop, H. F., Effect of an Adiabatic Fin on the Mixed Convection Heat Transfer in a Square Cavity with Two Ventilation Ports, *Thermal Science, 18,* (2014), 2, pp. 377-389
[21] Mahian, O., *et al.*, A Review of Entropy Generation in Nanofluid Flow, *International Journal of Heat and Mass Transfer,* 65, (2013), Oct., pp. 514-532
[22] Salari, M., *et al.,* Mixed Convection of Nanofluid Flows in a Square Lid-Driven Cavity Heated Partially from Both the Bottom and Side Walls, *Num. Heat Transfer, Part A, 62* (2012), 2, pp. 158-177
[23] Brinkman, H. C., The Viscosity of Concentrated Suspensions and Solution, *J. Chemical Physics 20* (1952), 4, pp. 571-581
[24] Abu-Nada, E., Chamkha, A. J., Effect of Nanofluid Variable Properties on Natural Convection in Enclosures, *International Journal of Thermal Science, 49* (2010), 3, pp. 479-491
[25] Bejan, A., *Entropy Generation through Heat and Fluid Flow*, Wiley, New York, N. Y., USA, 1982
[26] Patankar, Von S. V., *Numerical Heat Transfer and Fluid Flow,* Hemisphere Publishing Corporation, McGraw Hill Book Company, New York, N. Y., USA, 1980
[27] Abu-Nada, E., Chamkha, A. J., Mixed Convection Flow in a Lid-Driven Inclined Square Enclosure Filled with a Nanofluid, *Eur. J. Mech. B/Fluids, 29* (2010), 6, pp. 472-482
[28] Iwatsu, R., *et al.*, Mixed Convection in a Driven Cavity with a Stable Vertical Temperature Gradient, *Int. J. Heat Mass Trans., 36* (1993), 6, pp. 1601-1608
[29] Khanafer, K., Chamkha, A. J., Mixed Convection Flow in a Lid-Driven Enclosure Filled with a Fluid-Saturated Porous Medium, *Int. J. Heat Mass Trans., 42* (1999), 13, pp. 2465-2481
[30] Davis, de Vahl G., Natural Convection of Air in a Square Cavity: a Bench Mark Numerical Solution, *Int. J. Num. Methods Fluids, 3* (1983), 3, pp. 249-264
[31] Magherbi, M., *et al.*, Entropy Generation at the Onset of Natural Convection, *Int. J. Heat and Mass Trans., 46* (2003), 18, pp. 3441-3450
[32] Oztop, H. F., *et al.*, Computational Analysis of Non-Isothermal Temperature Distribution on Natural Convection in Nanofluid Filled Enclosures, *Science Direct, Superlattices and Microstructures, 69* (2011), 4, pp. 453-467

Paper submitted: February 1, 2013
Paper revised: March 7, 2015
Paper accepted: March 20, 2015